Wind Tunnel Testing of Wings in Spin

Adam M. Ragheb[*] and Michael S. Selig[†]

Experimental wind tunnel tests were conducted in the University of Illinois at Urbana-Champaign low-speed low-turbulence wind tunnel to study the aerodynamics of stalled spinning wings. Wings with airfoils of $t/c \approx 10\%$ and aspect ratios between 1 and 10 were tested at pitch angles of 30, 60, and 90 deg. In addition, the effects of airfoil shape were investigated by testing wings with symmetric, flat-bottom, and flat-plate airfoils. Results for Reynolds numbers between 3,000 and 25,000 show that the normal force coefficient C_N increases both with higher aspect ratio and higher nondimensional spin rate ($\omega = \Omega b/2V$). The effect of wing aspect ratio was observed to decrease as the wing pitch angle was increased within the stall regime to 90 deg. No Reynolds number effects were observed over the range of Reynolds numbers tested. The normal force coefficient C_N was observed to follow the square of ω within the range of spin parameter values that may be experienced by an aircraft in a stall/spin situation. For high spin parameter values, a change in concavity was observed, indicating the existence of a C_N plateau. A C_N plateau value, which increases with the aspect ratio, was measured for $Æ\!R = 1$ and $Æ\!R = 2$ wings. Flat-bottom airfoils exhibited larger C_N values than symmetric airfoils, but no significant difference was observed between flat-plate and flat-bottom airfoils.

Nomenclature

A	=	area of swept disc of wing in spin
b	=	wing span
c	=	chord length
$\bar{c}$	=	wing mean aerodynamic chord
C	=	test section cross-sectional area
C_D	=	drag coefficient
C_l	=	sectional lift coefficient
C_N	=	normal force coefficient
D	=	drag force
$k_{fairing}$	=	velocity correction factor due to fairing
q	=	dynamic pressure
R_s	=	spin radius
Re	=	Reynolds number based on mean aerodynamic chord
Ro	=	Rossby number
S_W	=	wing reference area
t	=	airfoil thickness
$V_{c_{fairing}}$	=	weighted average of velocities across spinning wing area
V_C	=	free air velocity
V_∞	=	freestream velocity
α	=	ratio of spinning wing swept area to test section cross-sectional area (A/C)
θ	=	pitch angle
μ	=	kinematic viscosity
ρ	=	air density
τ	=	drag force coefficient of spinning wing ($D/\rho A V_\infty^2$)
ω	=	spin parameter ($\Omega b/2V$)
Ω	=	angular velocity about axis of spin

[*]Ph.D. Candidate, University of Illinois at Urbana-Champaign, Department of Aerospace Engineering, 104 S. Wright St., Urbana, IL 61801, AIAA Student Member

[†]Professor, University of Illinois at Urbana-Champaign, Department of Aerospace Engineering, 104 S. Wright St., Urbana, IL 61801, AIAA Associate Fellow

American Institute of Aeronautics and Astronautics

$\mathcal{R}$ =   aspect ratio

Acronyms

FSTD   =   flight simulator training device
LEV   =   leading edge vortex
PIV   =   particle image velocimetry
UPRT   =   upset prevention and recovery training

I. Introduction

Research into the aerodynamics of stall/spin has been a topic of ongoing interest since as early as the 1930s,[1–3] and any improvements in aircraft stall/spin behavior have the potential to save many lives. Accidents in which stall/spin are cited account for about 7% of total pilot-related single-engine accidents, yet these accidents represent a staggering 65–70% of the total number of fatalities.[4] The only deadlier causal factor cited in accidents is weather, which is cited in only 5–6% of total pilot-related single-engine accidents but is a factor in 65–75% of the fatalities. For the purpose of clarity, multiple causal factors are often cited in aircraft accidents.[4]

Interest in the study of stall/spin has recently been renewed through the release of a final rule by the Federal Aviation Administration (FAA) mandating the incorporation of an extended envelope into Flight Simulator Training Devices (FSTDs) within 5 years of its release as part of training for Upset Prevention and Recovery Training (UPRT).[5] A subsequent proposed update to this final rule states that if a simulator used for post-stall flight training is inaccurate in the upset regime, the pilot may learn control strategies in the simulator that are inappropriate or potentially dangerous.[6]

The stall/spin characteristics of general aviation aircraft was studied by NASA in the late 1970s and early 1980s, and a large amount of rotary balance data was generated from these experiments.[7–19] All of these rotary balance data showed that as the spin rate increased, the wing normal force coefficient C_N grew roughly proportional to the square of the spin parameter ω. In 1981, McCormick[20] reported that a simple strip analysis is unable to predict these effects of the spin rate on the wing normal force. As a correction to this strip analysis, McCormick introduced a model[20] that accounts for the radial pressure gradient (centrifugal pumping of the spanwise flow) to obtain better estimates of the significant increase in the wing normal force coefficient C_N with increasing spin rate.

A key nondimensional parameter that defines the aerodynamics of wings in spin is the spin parameter defined as

$$\omega = \frac{\Omega b}{2V_\infty} \tag{1}$$

where b is the wing span, Ω is the angular velocity about the spin axis, and V_∞ is the freestream velocity. Typically, low values of ω correspond to a steep spin with the aircraft pitched with its nose toward the ground, while ω values above 0.9 correspond to a flatter spin mode where the nose is pointing in a nearly-horizontal direction.[21] Flight spin parameter values typically do not exceed $|\omega| = 1$, and thus the NASA general aviation rotary balance tests in the 70's and 80's were conducted for $|\omega| \leq 1$. In a more recent test, the Boeing Blended-Wing-Body was tested at a spin parameter value of $\omega = 0.67$.[22] In regards to the spin radius, a very small spin radius R_s is typical and generally on the order of $0.06b < R_s < 0.20b$.[21]

The increased C_N on a wing in spin is a phenomenon that is also observed in the insect and MAV fields of research, and experimental investigations into insect and flapping wing flight have provided insight into the structures and forces associated with wings in spin. Experiments by Lentink and Dickinson[23] showed that a unidirectionally translating fly wing in a tank filled with either oil or water produced a maximum C_D of around 1.5 in the regime $110 < Re < 14,000$. When the wing motion was changed to unidirectionally revolving (akin to an airplane spin), C_D values of between 3 and 4 were measured. In the experiments, the wings and plates were attached at one of their tips, as opposed to having the wing centered on the rotational axis. The trends of higher coefficent data found in these experiments is supported by numerical simulations. Garmann[24] analyzed flat plates ($\mathcal{R} = 1, 2,$ and 4) and showed local sectional lift coefficients of around $C_l = 2.5$ and wing drag coefficients of $C_D \approx 3.0$.

An important number for stalled wings in spin is the Rossby number Ro. This dimensionless parameter is a measure of the ratio of the inertial and centrifugal forces to the Coriolis force, and for a spinning wing it is defined by[23]
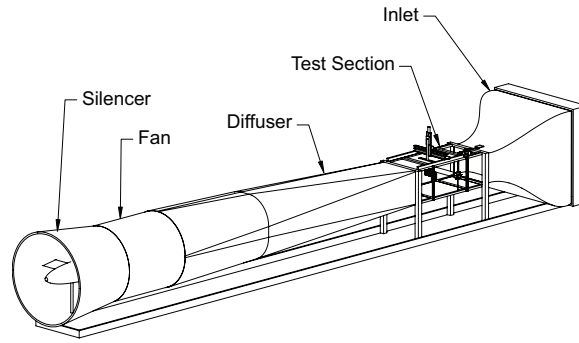
American Institute of Aeronautics and Astronautics

Figure 1. University of Illinois 2.8 × 4.0 ft low-speed low-turbulence wind tunnel.

$$Ro = \frac{R_g}{\bar{c}} \tag{2}$$

where R_g is the radius of gyration and $\bar{c}$ is the mean aerodynamic chord. Lentink and Dickinson[23] suggest a simplification of Ro where it is calculated with respect to the wingtip radius by

$$Ro = \frac{b}{2\bar{c}} \tag{3}$$

which is equal to the aspect ratio of a half-wing, or one half the aspect ratio of a wing. Observations by Lentink and Dickinson[23] noted that for low local Rossby numbers (e.g., $Ro < 3$ as defined by Eq. 3), a strong leading edge vortex (LEV) dominates the flow structures, and serves as a channel for pumping fluid outward along on the span. This LEV structure is not the only channel for radially pumped fluid, which has been shown to extend to the wing trailing edge.[25–27]

The purpose of this study is to parametrically identify the various effects of Reynolds number, aspect ratio, and airfoil geometry on the relationship between the spin parameter ω and the normal force coefficient C_N for wings in spin with $R_s = 0$. These investigations support the larger objective of the present work, which is to validate an analytical model of the wing normal force of an airplane for use in simulating the aerodynamics stalled and spinning, e.g. such as that methodology presented in Refs. 28 and 29 .

This paper is divided into five sections. The experimental setup is described in Section II and the wing test article properties are presented in Section III. The experimental results are plotted and discussed in Section IV, and the conclusions are presented in Section V.

II.   Experimental Setup

This section discusses the experimental setup, wind tunnel corrections used, motion control system, and data acquisition setup of these experiments. Aerodynamic tests of wings in spin were conducted in the University of Illinois at Urbana-Champaign low-speed low-turbulence subsonic wind tunnel shown in Fig. 1. The open-return tunnel has an inlet contraction ratio of 7.5:1, and the rectangular test section is 2.8×4.0 ft (0.853×1.22 m) and is 8 ft (2.44 m) long. The width of the test section increases by approximately 0.5 in (1.27 cm) to account for boundary layer growth at the test section sidewalls. To ensure good flow quality in the test section, one 4-in (10.2 cm) thick honeycomb and four anti-turbulence screens are located in the settling chamber. The empty-tunnel turbulence intensity is less than 0.1% for all operating conditions, which is sufficient for low Reynolds number airfoil measurements.[30,31] The maximum empty-test-section speed is 235 ft/s (71.5 m/s), although the tunnel was operated at speeds up to only 35 ft/s (10.7 m/s) in the current research. The test section speed was set by a 125 hp (93.2 kW) AC motor driving a five-bladed fan controlled by an ABB ACS 800 low-voltage AC drive. The test-section speeds were measured with an MKS 220 1-torr differential pressure transducer connected to static ports in the settling chamber and at the inlet of the test section. Ambient pressure was measured with a Setra Model 270 pressure transducer. With these pressure transducers, the test section speed was computer-controlled to within 1% of the prescribed speed.

The normal force was determined through the use of the drag balance shown in Figs. 2–3, which pivoted on two sealed ball bearings and was constrained on the downstream side by a load cell.[32] The propeller rig described in Ref. 33 was modified by reversing the streamwise orientation of the load cell and by replacing the flexures with ball
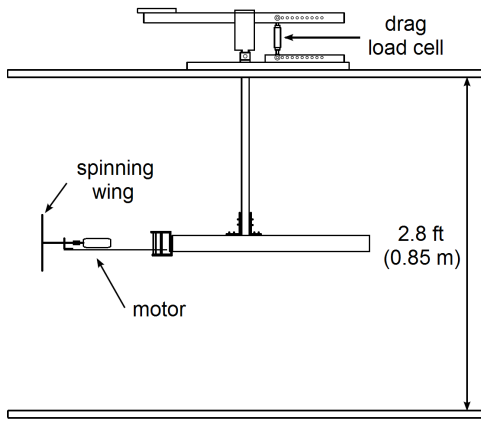
American Institute of Aeronautics and Astronautics

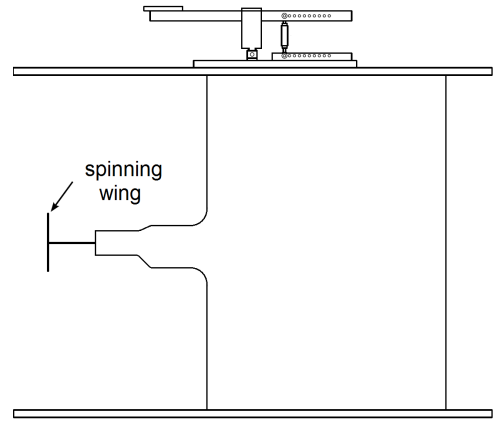**Figure 2. Experimental setup for drag force measurement (fairing not shown).**

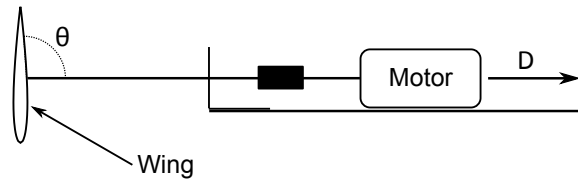**Figure 3. Spinning wing balance enclosed in fairing.**

Figure 4. Diagram of experimental spinning wing setup showing the wing location, orientation of θ, motor location, and direction of D.

bearings to account for the higher loads. An Interface SMT S-type load cell with a load capacity of 10 lb (44 N) was used to measure the drag force experienced by the rotating wing.

The drag load cell could be located at one of ten different locations in 0.5 in (1.27 cm) increments, ranging from 3.25 in (8.26 cm) to 7.75 in (19.69 cm) from the pivot point. These ten locations allowed the length of the moment arm to be changed to allow for the full measurement range of the load cell based on the measured drag. The weight and resulting force of the motor and sting structure maintained the load cell in tension for all test cases, ensuring that a negative drag condition, which could cause slipping of the load cell, was prevented. The normal force coefficient was determined from the drag of the spinning wing with the assumption that the net rotating lift component was small in comparsion with the drag. Thus, using $D \gg L$ yields

$$C_N \approx \frac{D}{qS_W} \sin\theta \tag{4}$$

where D is the drag force exerted on the spinning shaft, q is the dynamic pressure, S_W is the wing area, and θ is the pitch angle of the wing. Figure 4 depicts a detailed view of the spinning wing and motor of Fig. 2, with the wing, the orientation of θ, the motor, and the direction of the drag force labeled. Figure 5 depicts the relative orientations of V_∞, D, and C_N based on θ as used in Eq. 4. The Reynolds number of a wing in these tests was defined by the freestream velocity and mean aerodynamic chord, i.e.

$$Re = \frac{\rho V_\infty \bar{c}}{\mu} \tag{5}$$

where the viscosity μ was determined via Sutherland's law from the ambient temperature as measured by an Omega type-K static-temperature thermocouple.

A NACA 0025 symmetric fairing of chord length 24 in (0.61 m) was used to keep the motor sting, balance support arm, motor motion controller, and associated cabling out of the flow. This fairing, depicted in Fig. 6, spanned the entire test section from floor-to-ceiling in order to maintain a symmetric test section. The motor sting placed the rotating
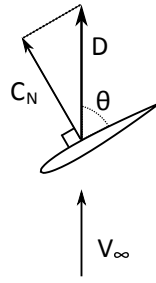
American Institute of Aeronautics and Astronautics

Figure 5. Diagram depicting relative orientations of V_∞, D, and C_N from Eq. 4.
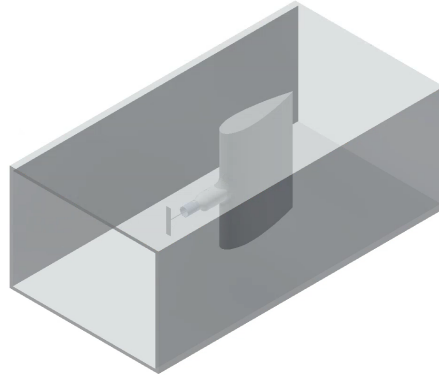

Figure 6. Isometric view of the fairing, sting, and spinning wing in the wind tunnel test section.

test specimen 17.75 in (44.45 cm) forward of the fairing leading edge – a sufficient distance forward to ensure that all wings in spin were over 1.7 wingspans upstream of the fairing. This forward placement of the wing in spin is based upon the forward placement of a propeller, which must be located at least 1.5 propeller diameters upstream of the fairing in order to minimize the effects on the wake structure behind the rotating body.[33]

A.   Wind Tunnel Corrections

Two wind tunnel corrections were used to correct the force data from testing the wings in spin. A velocity correction factor was used to account for the effect of a spinning wing in front of a fairing, and the Glauert[34,35] propeller correction was used to correct drag measurements. Testing a spinning wing, or any aerodynamic test article, in front of a fairing will result in the fluid velocity at the test article being lower than that measured at the wind tunnel test section entrance because the test article lies on or in the vicinity of the stagnation streamline. Since the wings are tested on a sting in front of a fairing, the fluid velocity at the wing will be less than the velocity measured at the beginning of the test section. To account for this reduction in velocity, the ratio of the velocities defines a correction factor, that is

$$\frac{V_{c_{fairing}}}{V_\infty} = k_{fairing} \tag{6}$$

where the value of the factor $k_{fairing}$[33,35] was determined for each wing based on the wing dimensions and the distance upstream of the fairing. Wall effects were assumed to be negligible because the spinning wings were small compared with the tunnel test section dimensions. Equation 6 uses a weighted average of the velocities experienced by the entire area of the spinning wing based on the distance forward of the fairing and the wingspan to determine the single velocity reduction factor.[33]

The Glauert[34,35] correction for testing propellers in a closed wind tunnel test section was used to correct the spinning wing drag data. This velocity correction is used to correct for testing thrust-producing propellers in a closed test section, as constraining a thrust-producing propeller or a drag-producing wing in spin to a closed test section yields a difference from testing that article in free air. A spinning wing producing drag will have a wake region immediately downstream of the wing with a velocity lower than the nominal wind tunnel test section velocity. In order to maintain

American Institute of Aeronautics and Astronautics

a constant mass flux of air (i.e., satisfy continuity) both upstream and downstream of the spinning wing, the region outside of the wake must be at a higher velocity than the freestream. Thus, the pressure outside of the wing wake would be lower than that upstream of the spinning wing, and thus the drag measured is higher than what would be measured in free air for that same velocity. In other words, the drag measured would occur at a lower velocity in free air, and that lower velocity may be determined from

$$\frac{V_c}{V_\infty} = 1 - \frac{\tau\alpha}{2\sqrt{1+2\tau}} \tag{7}$$

where α is the ratio of the swept area of the spinning wing and the test section cross-sectional area, and

$$\tau = \frac{D}{\rho A V_\infty^2} \tag{8}$$

The correction given by Eq. 6 and the Glauert correction for testing a propeller in a closed test section (Eq. 7) were applied to all data, and the accuracy was verified based on calibration runs of non-rotating wings of varying $\mathcal{R}$ compared with the C_D vs. $1/\mathcal{R}$ data of Ref. 36.

B.   Motion Control and Data Acquisition

The wings were rotated using a Faulhaber 3268G024BX4AES-4096 brushless DC servomotor which was controlled by an MCBL 3006 AES-series motion controller connected via a RS232 cable to a computer running the Faulhaber Motion Manager 5.1 software. This software allowed for the motor rotational speed to be set to and maintained at specific RPM values and monitored in realtime. The 3268 series DC servomotor has an operating range of 0 to 11,000 RPM and is capable of a maximum torque of 92 mN·m. Shaft position information was measured by an absolute encoder and provided to the motion controller at a resolution of 4096 steps per revolution via a serial (SSI) interface. Power was supplied to the DC-servomotor by an NEC NG-150642-001 24-V 600-mA power supply that was connected to the controller.

All instrumentation voltages were channeled to a National Instruments PCI-6031E 16-bit analog-to-digital data acquisition (DAQ) board that was connected to a personal computer upon which the data were recorded. A LabVIEW program was used to record the drag, dynamic pressure, atmospheric pressure, and temperature at 3,000 Hz for a duration of 3 sec, and these data were subsequently time averaged to yield one steady state value returned to the computer. Each wind tunnel run was conducted at a constant freestream velocity, and the motor speed was varied to produce the desired range of spin parameter ω values. The motor speed was controlled to within 1% during the recording time period.

III.   Wing Test Article Properties

Three types of wings were tested in this experiment including carbon fiber symmetric wings with a foam core, solid plastic flat bottom wings, and 3 mm plywood flat plate wings. All of the symmetric carbon fiber airfoils had a thickness-to-chord ratio of around 10%. These spinning wing test articles were made using a 3/16 in (4.76 mm) diameter steel shaft and symmetric radio-controlled helicopter blades. The test articles were linked to the 5 mm shaft of the motor with a 3/16 in to 5 mm bellows coupling to account for minor shaft misalignments. Holes were drilled in the wings to accept the shaft that was mounted at pitch angles (θ) of 30, 60, and 90 deg (see Fig. 4 defining the pitch angle). The shaft was glued to the wing with epoxy so that its tip was flush with the forward-facing surface of the wing.

The dimensions and information for the five blades used in the study of wing aspect ratio effects are summarized in Table 1, which presents the $\mathcal{R}$, chord length, wingspan, and area of each of the wings. Figure 7 presents a CAD rendering of the $\mathcal{R} = 4.85$ wing test articles at 90, 60, and 30 deg orientations. The area of each wing was held as close as practical to 13 in^2 (84 cm^2) and resulted in a range of aspect ratios that included and expanded beyond values that would be seen on a typical general aviation aircraft.

Additional tests were carried out on homogeneous, solid plastic blades, and on flat plate wings constructed from 3 mm plywood. Both of these wing styles were constructed in the same manner as the symmetric carbon fiber wings. The plastic blades were selected because their uniform density made them capable of higher rotation speeds which allowed a greater range of ω values to be studied. Additionally, blades of similar chord lengths were available with symmetric and flat-bottom airfoils which allowed for the effects of airfoil shape to be investigated. Table 2 presents information on these flat bottom airfoil and flat plate wings.

Table 1. Aspect Ratio Study Wing Blade Information and Dimensions

Aspect Ratio	Raw Blade	Chord Length	Wingspan	Area
8.33	Align 325D 325 mm	1.25 in (3.2 cm)	10.4 in (26.4 cm)	13.0 in^2 (83.9 cm^2)
6.50	KBDD 32W 325 mm	1.37 in (3.5 cm)	8.91 in (22.6 cm)	12.2 in^2 (78.8 cm^2)
4.85	Revolution RVOB043000 430 mm	1.65 in (4.2 cm)	8.00 in (20.3 cm)	13.2 in^2 (85.2 cm^2)
3.85	KBDD 350W 350 mm	1.85 in (4.7 cm)	7.13 in (18.1 cm)	13.2 in^2 (85.1 cm^2)
2.55	Pro3D DY-6001 600 mm	2.20 in (5.6 cm)	5.61 in (14.2 cm)	12.3 in^2 (79.6 cm^2)

Table 2. Airfoil Shape Study Wing Blade Information and Dimensions

| Aspect Ratio	Raw Blade	Chord Length	Wingspan	Area
5.97	HDX VTS-109Y (flat-bottom)	1.35 in (3.4 cm)	8.06 in (20.5 cm)	10.9 in^2 (70.2 cm^2)
6.30	HDX VTS-108Y (symmetric)	1.14 in (2.9 cm)	7.19 in (18.3 cm)	8.19 in^2 (52.9 cm^2)
1.00	3mm plywood (flat plate)	3.63 in (9.2 cm)	3.63 in (9.21 cm)	13.1 in^2 (84.8 cm^2)
2.00	3mm plywood (flat plate)	2.50 in (6.4 cm)	5.00 in (12.7 cm)	12.5 in^2 (80.7 cm^2)
5.00	3mm plywood (flat plate)	1.50 in (3.8 cm)	7.50 in (19.1 cm)	11.3 in^2 (72.6 cm^2)
10.0	3mm plywood (flat plate)	1.19 in (3.0 cm)	11.9 in (30.2 cm)	14.1 in^2 (91.0 cm^2)
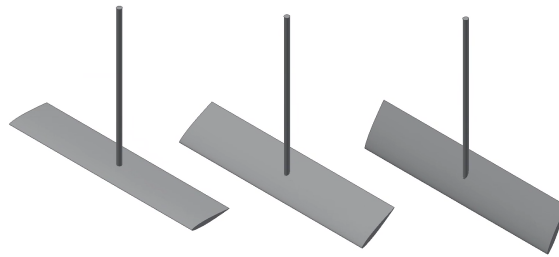
Figure 7. CAD rendering of the $\mathcal{R} = 4.85$ wing of Table 1 at 90, 60, and 30 degree orientations, left to right.

After each test article was assembled, it was statically balanced along the span. This static balancing was achieved through a combination of removing any preexisting counterweights from inside the wing and affixing small steel bolts and drops of epoxy into the foam core at the wingtip. For the 90 deg blades, the hole for the steel shaft was drilled at the 50% chord location because in a heavily-stalled situation the lift vector acts near that location. For the 30 and 60 deg blades, the shaft was located as close as possible to passing through the 50% chordline despite the fact that structural considerations had to be the primary driver of the hole drilling location.

IV. Results and Discussion

In this section the experimental results of testing stalled spinning wings in a wind tunnel are presented. This section will parametrically establish the effect of Reynolds number, aspect ratio, airfoil geometry, and high spin parameter values.

A. Reynolds Number Effects

The first investigation was performed to establish the effect of Reynolds number upon the aerodynamic flowfield of stalled spinning wings. It has been well established that minimal Reynolds number effects exist on unswept non-yawing wings in the post-stall regime, but the literature is devoid of any information on stalled wings in spin in regards to Reynolds number effects. To investigate whether or not Reynolds number effects exist on stalled wings in spin, a number of wings were tested at different Reynolds numbers.
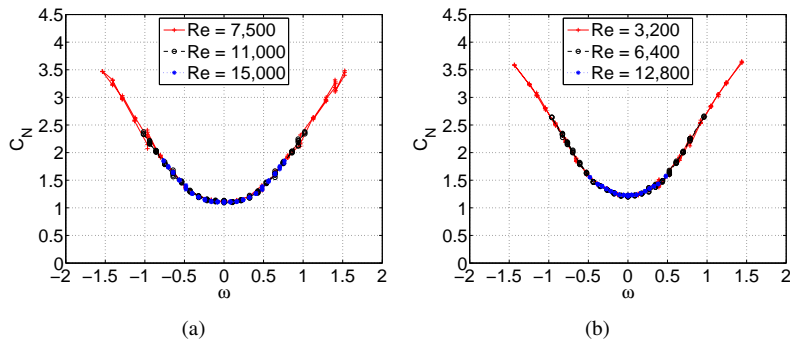
American Institute of Aeronautics and Astronautics

Figure 8. ω versus C_N for three different Re values at $\theta = 90$ deg for a symmetric wing with (a) $\mathcal{R} = 6.50$, and (b) a flat plate with $\mathcal{R} = 5.00$.
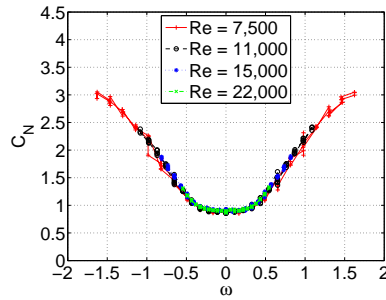

Figure 9. ω versus C_N for a symmetric wing at three different Re values at $\theta = 60$ deg for a wing with $\mathcal{R} = 2.55$.

Figure 8(a) presents C_N data for the $\mathcal{R} = 6.50$ wing at $\theta = 90$ for three different freestream Reynolds numbers. By coplotting the data in this manner, it is evidenced that no Reynolds number effects exist for a stalled spinning wing over the range of Reynolds numbers tested. This is significant because the previous state of the literature only addresses stalled, unspinning wings. These data demonstrate that the addition of rotation to a stalled wing does not add a Reynolds number dependency within the range of Reynolds numbers tested in this research. This lack of a Reynolds number dependency is further supported by Fig. 8(b) which presents data for the $\mathcal{R} = 5.0$ flat-plate wing at $\theta = 90$ deg and at three different Reynolds numbers. Across the Reynolds number range, the C_N data follow the same ω^2 relationship with no offset or change in the rate of growth.

To further investigate Reynolds number effects at slightly higher Reynolds numbers, a low aspect ratio wing of $\mathcal{R} = 2.55$ was tested at $\theta = 60$ deg. The data for this wing are presented in Fig. 9. As shown, no Reynolds number effects are apparent across a range of Reynolds number and pitch angles. This suggests that the 3D flow structures present in a stalled spinning wing are the same across the range of Reynolds numbers tested. For a constant maximum attainable rotation speed, an increased Reynolds number results in a decrease in the maximum attainable ω value. However, the benefit of testing at higher Reynolds numbers is an increased resolution in ω and decreased variation in the range of ω values very close to zero. As shown in Fig. 9, the $Re = 22,000$ data points provide smooth and finely-spaced data centered around $\omega = 0$, and these data do not differ from those of the lower Reynolds numbers.

It is also observed in Fig. 9 that the $C_N - \omega$ plot appears to exhibit a decreased C_N growth rate for $|\omega| > 1$, suggesting the presence of a maximum attainable C_N value. (An investigation into high values of ω with a flat-bottom wing of $\mathcal{R} = 5.97$ at $\theta = 90$ deg is presented later in Fig. 12(b).) While the trend in Fig. 9 changes concavity for $|\omega| > 1$ and $C_N \approx 2.5$, the data of Fig. 12(b) changes concavity for $|\omega| > 1.6$ and $C_N \approx 4$. These data suggest that this maximum attainable C_N may have an $\mathcal{R}$ dependency as will be explained later in Section IV D. The majority of tests were conducted in the $|\omega| < 1$ regime, as that is within the expected range of a spinning aircraft. If an aircraft were to be spinning at $\omega = 3$, other considerations would become more important than the aerodynamics, as it would be expected that a structural limit on the wings or a biological limit on the occupants would have already been reached and exceeded in that spin regime.
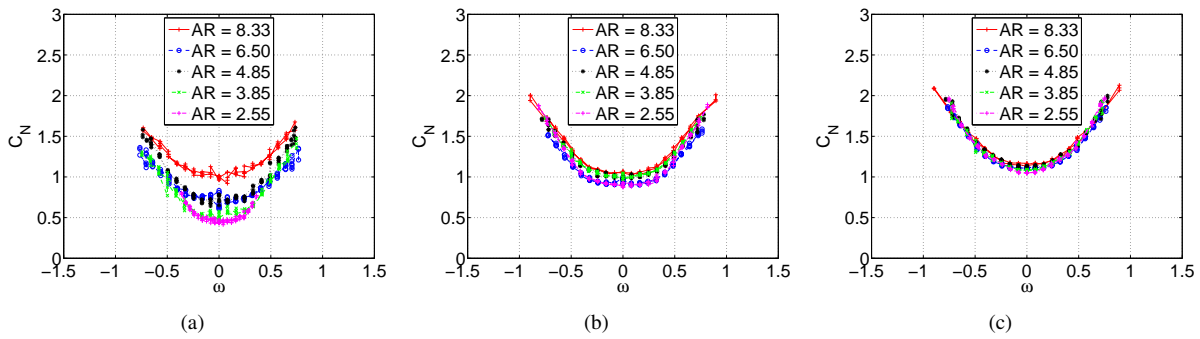
American Institute of Aeronautics and Astronautics

Figure 10. ω versus C_N for five different $\mathcal{R}$ values for a symmetric wing at $Re = 15,000$ and (a) $\theta = 30$ deg, (b) $\theta = 60$ deg, and (c) $\theta = 90$ deg.

Figure 11. ω versus C_N for five different $\mathcal{R}$ values for a symmetric wing at $Re = 11,000$ and (a) $\theta = 30$ deg, (b) $\theta = 60$ deg, and (c) $\theta = 90$ deg.
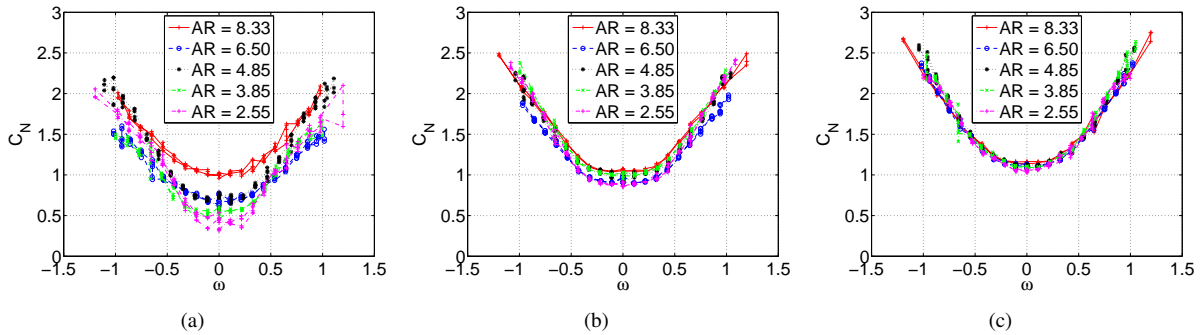
B. Aspect Ratio Effects

To investigate the effects of the wing aspect ratio on C_N across the range of ω, the five wing planforms of Table 1 were tested at pitch angles of 30, 60, and 90 deg. Time-averaged data for the wing normal force of the five different aspect ratio wings were acquired over the approximate range of $-1 < \omega < 1$ at various Reynolds numbers. Data for $Re = 15,000$ are presented in Fig. 10 for pitch angles of 30, 60, and 90 deg, and data at $Re = 11,000$ are presented in Fig. 11 for the same pitch angles. As visible in Figs. 10 and 11, C_N is generally proportional to the square of ω for all values of θ. Also evident in Figs. 10 and 11 is that as the wing pitch angle θ increases from 30 to 90 deg, the curves for the different $\mathcal{R}$ wings exhibit smaller differences between one another, and all increase in magnitude. This increase in C_N is more prevalent for the lower $\mathcal{R}$ wings. While the C_N value at $\omega = 0$ for the $\mathcal{R} = 2.55$ wing increases by 0.62 from 0.43 in Fig. 10(a) to 1.05 in Fig. 10(c) as θ is increased from 30 to 90 deg, the C_N value of the $\mathcal{R} = 8.33$ wing only increases by 0.18 from 0.99 to 1.17 for the same change in θ. Thus, the effect of aspect ratio, which is present to some degree at all θ values, is increased as the pitch angle θ is decreased. This is due to the fact that, as the wing pitch angle is decreased, the wing is being operated in a condition closer to an unstalled state. Because the wing is nearer to an unstalled state, differences induced by aspect ratio, such as wingtip vortices, downwash, and the resulting change in performance, are more pronounced.

While all the curves generally demonstrate a similar relationship between ω and C_N, it is of note that the C_N values for the $\mathcal{R} = 2.55$ and 3.85 wings grow noticeably more rapid with ω than the higher aspect ratio wings for values of $|\omega| < 0.5$ and $\theta = 30$ deg as shown in Fig. 10(a). In the case of a low aspect ratio wing at a moderate spin parameter, the Coriolis forces dominate the centrifugal forces, the former of which tend to push the wake region off of the aft edge of the airfoil. This increased rate of C_N growth for the low aspect ratio wings is attributable to a leading edge vortex (LEV) structure serving as a channel for centrifugally-pumped fluid that forces part or all of the tip vortex structures outboard of the wingtip. By pushing any tip vortex structures outboard and away from the wing, the wake structure is able to be larger and unencumbered by any downwash-producing structures which results in a more rapid growth of C_N. At lower aspect ratios, less of the spanwise flow is pushed off of the wing trailing edge, and thus more flow is available to push the tip structures outboard. This agrees with the observations of Ref. 23 in which a strong leading
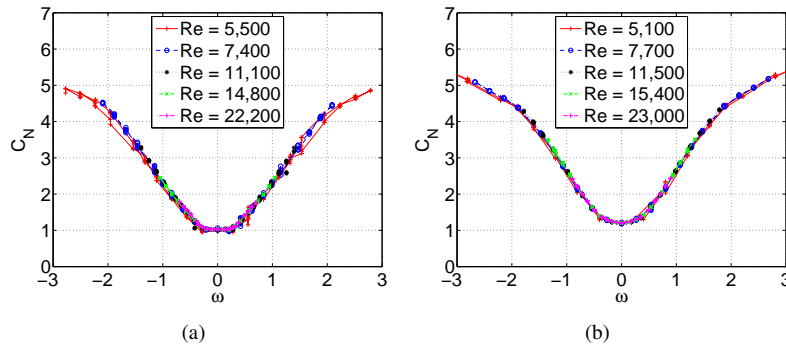
Figure 12. ω versus C_N for five different Re values at $\theta = 90$ deg for (a) a symmetric wing with $\mathcal{R} = 6.30$, and (b) a flat-bottom wing with $\mathcal{R} = 5.97$.

edge vortex was observed to dominate the flow structures and serve as a channel for pumping fluid outward along the span.

C. Airfoil Geometry Effects

Figure 12 presents C_N versus ω data for a symmetric airfoil wing with $\mathcal{R} = 6.30$ and a flat-bottom airfoil wing of $\mathcal{R} = 5.97$. While the C_N values for the flat-bottom airfoil wing are slightly higher than those of the symmetric airfoil wing, the shape of both curves follows the ω^2 relationship over the range of the spin parameter tested. The data from both wings indicates a change in the concavity around $|\omega| \approx 1.6$, where the curve begins to flatten out. The data in Fig. 12 also confirm that, as expected, no significant qualitative differences exist between the stalled spinning wing testing of a flat plate versus a symmetric airfoil wing. No quantitative difference is observed between flat-bottom and flat-plate wings of similar aspect ratios, suggesting that it is only the flow-facing geometry that matters post-stall. The $\mathcal{R} = 5.97$ flat-bottom wing of Fig. 12(b) and the flat-plate wing of Fig. 8(b) both have C_N values of around 1.25 for $\omega = 0$, and their C_N curves generally have similar values.

A quantitative difference exists, however, between the symmetric airfoil wings and the flat-bottom airfoil wings. In Fig. 13, the $\mathcal{R} = 5.00$ flat plate wing at $\theta = 90$ deg has $C_N = 1.25$ at $\omega = 0$, while for the $\mathcal{R} = 4.85$ symmetric wing of Fig. 10(c), $C_N = 1.13$ at $\omega = 0$. This is due to the fact that the flat-plate and flat-bottom wings act as a pure bluff body while the symmetric wing acts more like a body with some degree of roundedness on its flow-facing side. This explanation is supported by experimental data for a wing with a flat-bottom airfoil and $\mathcal{R} = 5.97$, as shown in Fig. 12(b), aligning more closely with the flat-plate airfoil C_N values than for the symmetric airfoil C_N values.

D. High Spin Parameter Effects

Data for flat-plate wings of aspect ratios 1, 2, and 10 and a flat-bottom wing of aspect ratio 6 over the range of ω values $-5 < \omega < 5$ at $\theta = 90$ deg are presented in Fig. 13. As expected, for low spin parameter values, the C_N data for all wings follows the ω^2 relationship. Interestingly, data for the $\mathcal{R} = 1$ wing show that a maximum attainable, or plateau, C_N value of approximately 1.3 is reached for $|\omega| > 0.25$. In the case of the $\mathcal{R} = 2$ wing, C_N reaches a plateau value of approximately 1.9 for $|\omega| > 0.8$. The $\mathcal{R} = 6$ flat-bottom wing shows that a change in concavity occurs around $|\omega| = 1.6$ and $C_N \approx 4$. This change in concavity suggests that a C_N plateau value is being approached. When the wing aspect ratio is increased to 10 (see Fig. 13), this change in concavity occurs at $|\omega| \approx 3$ and $C_N \approx 6.6$, although once again spin parameter values large enough to reach the C_N plateau value were not attained.

The data of Fig. 13 clearly show evidence that a C_N plateau is present in a stalled spinning wing at which point further increasing the rotational rate of the wing will not affect C_N, and that this C_N plateau is aspect-ratio dependent. As the wing aspect ratio increases, the C_N plateau value, and the ω value at which that value is attained, both increase. For low aspect ratio wings, the increase in C_N is attributable to the presence of a leading edge vortex in which the vortex core produces spanwise flow supplied by Ekman-like pumping.[23] It is stressed that the local Rossby number is responsible for leading edge vortex stability; even on an $\mathcal{R} = 10$ wing, the inner 30% of the wing would experience a $Ro < 3$ irrespective of the Ro of the wing. As the wing aspect ratio increases, the influence of the leading edge vortex decreases and the influence of the entire wake region behind the wing extending from the leading edge to the trailing edge, which also experiences centrifugal pumping, is increased. As the spin parameter and aspect ratio are increased,
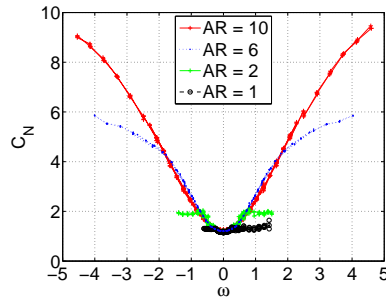
American Institute of Aeronautics and Astronautics

Figure 13. ω versus C_N for flat-bottomed wings of four different $A\!R$ values and $\theta = 90$ deg at various Re values.

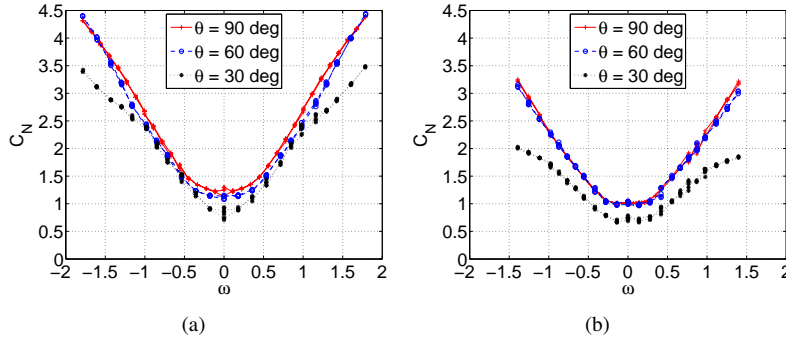(a)   (b)

Figure 14. ω versus C_N for three different θ values at $Re = 11,000$ for (a) a flat-bottom wing and (b) a symmetric wing.

the Coriolis force is increasingly able to push the wake structure and its radially-pumped fluid toward the trailing edge of the wing, thereby reducing the centrifugal pumping effects. However, for high values of ω, the outer portions of the wing are at lower angles of attack, thus reducing the size of the trapped wake structure and consequently further accelerating the spanwise flow. This acceleration of the spanwise flow reduces the effect of the Coriolis force trying to push the wake structure off of the back of the wing. At some point, however, the wake is pushed off of the wing trailing edge, and no further increase in C_N due to centrifugal pumping is possible. Additionally, as the rotational rate is further increased, the wing starts to unstall beginning at the tips. It is at this point that the C_N–ω curve flattens out. At low aspect ratios and high values of ω, the drag producing wake no longer takes the shape of the wing, but is thought to exist as a hemiellipsoid-shaped wake with the two shorter axes equal to the span of the wing, and the third, longer, axis extending downstream. Once the wake takes on the hemiellipsoid shape, its size and thus the drag produced by the spinning wing does not change as ω is further increased; this explains the C_N plateau observed in Fig. 13 for the aspect ratio 1 and 2 wings.

E.   Airfoil and High Spin Parameter Effects

The effects of airfoil shape at high values of ω are presented in Fig. 14 at $Re = 11,000$ and θ values of 30, 60, and 90 deg for a flat-bottom and symmetric wing. Overall, the flat-bottom wing exhibits higher C_N values than the symmetric wing for a given spin parameter at all θ values. Interestingly, the flat-bottom wing at $\theta = 30$ deg exhibits a significantly smaller dropoff relative to the 60 and 90 deg wings than the $\theta = 30$ deg symmetric wing.

At a spin parameter of unity, the $\theta = 30$ deg flat-bottom wing of Fig. 14(a) has a C_N slightly less than 2.5 and the $\theta = 60$ deg C_N value is just above 2.5. In contrast, the symmetric wing of Fig. 14(b) at $\omega = 1$ and $\theta = 30$ deg has $C_N = 1.5$ while the $\theta = 60$ deg $C_N = 2.25$. These data demonstrate that a flat-bottom wing has a slightly larger C_N value for a given ω than a symmetric wing, and that the decrease in C_N due to reducing θ is less-pronounced on flat-bottom wings. This increased performance of the lower-θ flat-bottom wing (or decreased decrease in C_N as θ is reduced) is hypothesized to be attributable in part to the presence of vortex lift. The sharper leading edge of the flat-bottom wing is thought to shed a more stable and stronger leading edge vortex. This stronger leading edge vortex helps keep the flow attached and serves as a channel for a portion of the spanwise flow, thus helping to reduce the

American Institute of Aeronautics and Astronautics

decrease in C_N compared with a symmetric, blunt-nosed wing, which would be characterized by a weaker leading edge vortex.

V. Conclusions

In this study, the effects of various parameters on the normal force coefficient of wings in spin were investigated. Well-developed methods for testing propeller performance were modified and adapted to research stalled spinning wings in a horizontal wind tunnel. The effects of Reynolds number, aspect ratio, airfoil geometry, and the spin parameter on the normal force coefficient C_N are summarized. For the regime tested, the Reynolds number was shown to have no effect, while an increase in the aspect ratio of a wing was shown to progressively increase the C_N value as the wing pitch angle θ was decreased; this was attributed to a decrease in the tip vortex effects of the higher aspect ratio wings as the wings approached an unstalled state. Flat-bottom and flat-plate wings were found to have slightly larger values of C_N than a symmetric airfoil for all values of ω, but no significant difference between a flat-bottom and flat-plate wing was observed. The slightly-larger C_N values of wings with a flat bottom were attributed to the flow-facing side acting more similar to a flat plate than a streamlined surface, and to a stronger leading edge vortex being shed by the sharp leading edge common to both the flat-plate and flat-bottom wings.

For high values of ω, well beyond those that would be expected for an airplane in a stall/spin situation, the data suggest that a maximum attainable C_N plateau value exists, and that this value increases as the wing aspect ratio is increased. This value is limited by the ability of lower local angles of attack, created by high spin parameter values, to reduce the size of the wake structure and further accelerate the spanwise flow, thus reducing the ability of the Coriolis forces to push the spanwise flow off of the wing trailing edge. When the lower local angles of attack are unable to prevent loss of the wake structure, a maximum C_N value is reached. This C_N plateau was reached for wings of $\mathit{\!R} = 1$ and $\mathit{\!R} = 2$, and at these low-aspect ratio conditions, the increased normal force is attributable primarily to centrifugal pumping in the leading edge vortex core as opposed to higher aspect ratio wings where the majority of the centrifugal pumping is experienced in the trapped wake structure.

These data may be used to validate analytic models of a wing in a stall/spin situation, which tends to drive the roll rate and normal force of a full-airplane configuration. These experimental data may thus aid in the development of simulations of aircraft that are well beyond the normal flight envelope, an area which has received recent regulatory attention. The experimental methodology that was derived from existing propeller testing methods shows promise for application to normal force measurements in a conventional wind tunnel on a spinning full-airplane (or at least fuselage-present) configuration as long as the model is properly balanced. Demonstrating that these tests may successfully be conducted in a conventional wind tunnel, as opposed to in a vertical wind tunnel, should help to make acquisition of similar data much easier as it requires less specialized equipment.

Acknowledgments

References

[1]Zimmerman, C. H., "Preliminary Tests in the NACA Free-Spinning Wind Tunnel," NACA Report 557, 1937.

[2]Soule, H. A. and Scudder, N. F., "A Method of Flight Measurement of Spins," NACA Report 377, 1931.

[3]Stephens, A. V., "Recent Research on Spinning," *Royal Aircraft Society Journal*, Vol. 37, No. 275, 1933, pp. 944–955.

[4]AOPA Air Safety Foundation, "Joseph T. Nall Reports (1997-2010)," http://www.aopa.org/asf/publications/nall.html, Accessed January 2012.

[5]Federal Aviation Administration, "14 CFR Part 121: Qualification, Service, and Use of Crewmembers and Aircraft Dispatchers; Final Rule," *Federal Register*, Vol. 78, No. 218, 2013.

[6]Federal Aviation Administration, "14 CFR Part 60: Flight Simulation Training Device Qualification Standards for Extended Envelope and Adverse Weather Event Training Tasks; Proposed Rule," *Federal Register*, Vol. 79, No. 132, 2014.

[7]Ralston, J. N., "Rotary Balance Data for a Typical Single-Engine General Aviation Design for an Angle-of-Attack Range of 8 to 90 deg: I - Influence of Airplane Components for Model D," NASA CR-3246, 1983.

[8]Barnhart, B., "Rotary Balance Data for a Typical Single-Engine General Aviation Design for an Angle-of-Attack Range of 8 to 90 deg: II - Influence of Horizontal Tail Location for Model D," NASA CR-3247, 1982.

[9]Bihrle, W., Barnhart, B., and Pantason, P., "Static Aerodynamic Characteristics of a Typical Single-Engine Low-Wing General Aviation Design for an Angle-of-Attack Range of -8 deg to 90 deg," NASA CR-2971, 1978.

[10]Bihrle, W., Hultberg, R. A., and Mulcay, W., "Rotary Balance Data for a Typical Single-Engine Low-Wing General Aviation Design for an Angle-of-Attack Range of 30 to 90 deg," NASA CR-2972, 1978.

[11]Mulcay, W. and Chu, J., "Rotary Balance Data for a Single-Engine Agricultural Airplane Configuration for an Angle-of-Attack Range of 8 to 90 deg," NASA CR-3311, 1980.

[12]Barnhart, B., "F-15 Rotary Balance Data for an Angle-of-Attack Range of 8 to 90 deg," NASA CR-3478, 1982.

[13]Bihrle, W. and Hultberg, R. S., "Rotary Balance Data for a Typical Single-Engine General Aviation Design for an Angle-of-Attack Range of 8 to 90 deg: I - High-Wing Model B," NASA CR-3097, 1979.

[14]Pantason, P. and Dickens, W., "Rotary Balance Data for a Single-Engine Trainer Design for an Angle-of-Attack Range of 8 to 90 deg," NASA CR-3099, 1979.

[15]Hultberg, R. S. and Mulcay, W., "Rotary Balance Data for a Typical Single-Engine General Aviation Design for an Angle-of-Attack Range of 8 to 90 deg: I - Low-Wing Model A," NASA CR-3100, 1980.

[16]Mulcay, W. and Rose, R. A., "Rotary Balance Data for a Typical Single-Engine General Aviation Design for an Angle-of-Attack Range of 8 to 90 deg: II - High-Wing Model A," NASA CR-3101, 1979.

[17]Mulcay, W. and Rose, R. A., "Rotary Balance Data for a Typical Single-Engine General Aviation Design for an Angle-of-Attack Range of 8 to 90 deg: I - Low-Wing Model C," NASA CR-3200, 1980.

[18]Hultberg, R. S., Chu, J., and Dickens, W. L., "Rotary Balance Data for a Typical Single-Engine General Aviation Design for an Angle-of-Attack Range of 8 to 90 deg: II - High-Wing Model C," NASA CR-3201, 1980.

[19]Bihrle, W. and Hultberg, R. S., "Rotary Balance Data for a Typical Single-Engine General Aviation Design for an Angle-of-Attack Range of 8 to 90 deg: II - Low-Wing Model B," NASA CR-3098, 1979.

[20]McCormick, B. W., "The Prediction of Normal Force and Rolling Moment Coefficients for a Spinning Wing," NASA CR-165680, February 1981.

[21]McCormick, B. W., *Aerodynamics, Aeronautics, and Flight Mechanics*, 2nd ed., John Wiley & Sons, Inc., New York, 1995, pp. 577–579.

[22]Vicroy, D. D., "Blended-Wing-Body Low-Speed Flight Dynamics: Summary of Ground Tests and Sample Results (Invited)," AIAA Paper 2009-0933, 47th AIAA Aerospace Sciences Meeting, Orlando, FL, 2009.

[23]Lentink, D. and Dickinson, M. H., "Rotational Accelerations Stabilize Leading Edge Vortices on Revolving Fly Wings," *The Journal of Experimental Biology*, Vol. 212, No. 16, 2009, pp. 2705–2719.

[24]Garmann, D. J. and Visbal, M. R., "Dynamics of Revolving Wings for Various Aspect Ratios," *Journal of Fluid Mechanics*, Vol. 748, 2014, pp. 932–956.

[25]Birch, J. M. and Dickinson, M. H., "Spanwise Flow and the Attachment of the Leading-Edge Vortex on Insect Wings," *Nature*, Vol. 412, 2001, pp. 729–733.

[26]Birch, J. M., Dickson, W. B., and Dickinson, M. H., "Force Production and Flow Structure of the Leading Edge Vortex on Flapping Wings and High and Low Reynolds Numbers," *The Journal of Experimental Biology*, Vol. 207, 2004, pp. 1063–1072.

[27]Lentink, D. and Dickinson, M. H., "Time-Resolved Reconstruction of the Full Velocity Field Around a Dynamically-Scaled Flapping Wing," *Experiments in Fluids*, Vol. 41, 2006, pp. 213–225.

[28]Selig, M. S., "Real-Time Flight Simulation of Highly Maneuverable Unmanned Aerial Vehicles," *Journal of Aircraft*, Vol. 51, No. 6, 2014, pp. 1705–1725.

[29]Ragheb, A. M. and Selig, M. S., "Improved Methodology for Predicting the Force on Stalled Spinning Wings," AIAA Paper 2015-0548, 53rd AIAA Aerospace Sciences Meeting, Kissimmee, FL, 2015.

[30]Selig, M. S. and McGranahan, B. D., "Wind Tunnel Aerodynamic Tests of Six Airfoils for Use on Small Wind Turbines," National Renewable Energy Laboratory, Technical Report NREL/SR-500-34515, Golden, CO, 2004.

[31]Khodadoust, A., "An Experimental Study of the Flowfield on a Semispan Rectangular Wing with a Simulated Glaze Ice Accretion," Ph.D. Thesis, University of Illinois at Urbana-Champaign, Department of Aeronautical and Astronautical Engineering, Urbana, IL, 1993.

[32]Brandt, J. B. and Selig, M. S., "Propeller Performace at Low Reynolds Numbers," AIAA Paper 2011-1255, 49th AIAA Aerospace Sciences Meeting, Orlando, FL, 2011.

[33]Deters, R. W., Ananda, G. K., and Selig, M. S., "Reynolds Number Effects on the Performance of Small-Scale Propellers," AIAA Paper 2014-2151, 32nd AIAA Applied Aerodynamics Conference, Atlanta, GA, 2014.

[34]Glauert, H., "Wind Tunnel Interference on Wings, Bodies and Airscrews," Aeronautical Research Committee, R&M No. 1566, 1933.

[35]Barlow, J. B., Rae, W. H., Jr., and Pope, A., *Low-Speed Wind Tunnel Testing*, 3rd ed., John Wiley & Sons, Inc., New York, 1999, pp. 433–435.

[36]Lindenburg, C., "Stall Coefficients," Energy Research Center of the Netherlands, ECN-RX-01-004, Petten, The Netherlands, IEA Symposium on the Aerodynamics of Wind Turbines, National Renewable Energy Laboratory, Golden, CO, December, 2000.